

# Boundary-Layer Theory

McGRAW-HILL SERIES IN MECHANICAL ENGINEERING

JACK P. HOLMAN, *Southern Methodist University*  
*Consulting Editor*

---

BARRON · *Cryogenic Systems*  
ECKERT · *Introduction to Heat and Mass Transfer*  
ECKERT AND DRAKE · *Analysis of Heat and Mass Transfer*  
ECKERT AND DRAKE · *Heat and Mass Transfer*  
HAM, CRANE, AND ROGERS · *Mechanics of Machinery*  
HARTENBERG AND DENAVIT · *Kinematic Synthesis of Linkages*  
HINZE · *Turbulence*  
JACOBSEN AND AYRE · *Engineering Vibrations*  
JUVINALL · *Engineering Considerations of Stress, Strain, and Strength*  
KAYS · *Convective Heat and Mass Transfer*  
LICHTY · *Combustion Engine Processes*  
MARTIN · *Kinematics and Dynamics of Machines*  
PIELAN · *Dynamics of Machinery*  
PIELAN · *Fundamentals of Mechanical Design*  
RAVEN · *Automatic Control Engineering*  
SCHENCK · *Theories of Engineering Experimentation*  
SCHLICHTING · *Boundary-Layer Theory*  
SHIGLEY · *Dynamic Analysis of Machines*  
SHIGLEY · *Kinematic Analysis of Mechanisms*  
SHIGLEY · *Mechanical Engineering Design*  
SHIGLEY · *Simulation of Mechanical Systems*  
STOECKER · *Refrigeration and Air Conditioning*

Dr. HERMANN SCHLICHTING

Professor Emeritus at the Engineering University of Braunschweig, Germany  
Former Director of the Aerodynamische Versuchsanstalt Göttingen

Translated by

Dr. J. KESTIN

Professor at Brown University in Providence, Rhode Island

Seventh Edition

McGRAW-HILL BOOK COMPANY

New York · St. Louis · San Francisco · Auckland · Bogotá ·  
Düsseldorf · Johannesburg · London · Madrid · Mexico · Montreal ·  
New Delhi · Panama · Paris · São Paulo · Singapore · Sydney · Tokyo · Toronto

### f. Comparison between the theory of perfect fluids and experiment

In the cases of the motion of water and air, which are the most important ones in engineering applications, the Reynolds numbers are very large because of the very low viscosities of these fluids. It would, therefore, appear reasonable to expect very good agreement between experiment and a theory in which the influence of viscosity is neglected altogether, i. e. with the theory of perfect fluids. In any case it seems useful to begin the comparison with experiment by reference to the theory of perfect fluids, if only on account of the large number of existing explicit mathematical solutions.

In fact, for certain classes of problems, such as wave formation and tidal motion, excellent results were obtained with the aid of this theory†. Most problems to be discussed in this book consist in the study of the motion of solid bodies through fluids at rest, or of fluids flowing through pipes and channels. In such cases the use of the theory of perfect fluids is limited because its solutions do not satisfy the condition of no slip at the solid surface which is always the case with real fluids even at very small viscosities. In a perfect fluid there is slip at a wall, and this circumstance introduces, even for small viscosities, such fundamental differences that it is rather surprising to find in some cases (e. g. in the case of very slender, stream-line bodies) that the two solutions display a good measure of agreement. The greatest discrepancy between the theory of a perfect fluid and experiment exists in the consideration of drag. The perfect-fluid theory leads to the conclusion that when an arbitrary solid body moves through an infinitely extended fluid at rest it experiences no force acting in the direction of motion, i. e. that its drag is zero (d'Alembert's paradox). This result is in glaring contradiction to observed fact, as drag is measured on all bodies, even if it can become very small in the case of a stream-line body in steady flow parallel to its axis.

By way of illustration we now propose to make some remarks concerning the flow about a circular cylinder. The arrangement of streamlines for a perfect fluid is given in Fig. 1.9. It follows at once from considerations of symmetry that the resultant force in the direction of motion (drag) is equal to zero. The pressure distribution according to the theory of frictionless motion is given in Fig. 1.10, together with the results of measurements at three values of the Reynolds number. At the leading edge, all measured pressure distributions agree, to a certain extent, with that for a perfect fluid. At the trailing end, the discrepancy between theory and measurement becomes large because of the large drag of a circular cylinder. The pressure distribution at the lowest, subcritical Reynolds number  $R = 1.9 \times 10^5$  differs most from that given by potential theory. The measurements corresponding to the two largest Reynolds numbers,  $R = 6.7 \times 10^5$  and  $R = 8.4 \times 10^6$ , are closer to the potential curve than those performed at the lowest Reynolds number. The large variation of pressure distribution with Reynolds number will be discussed in detail in the next chapter. A corresponding pressure-distribution curve around a meridian section of a sphere is reproduced in Fig. 1.11. Here, too, measurements show large differences for the two Reynolds numbers, and, again, the smaller Reynolds number lies in the range

† Cf. e. g. B. H. Lamb: Hydrodynamics, 6th ed., Dover, New York, 1945.

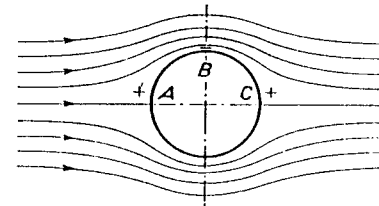


Fig. 1.9. Frictionless flow about a circular cylinder

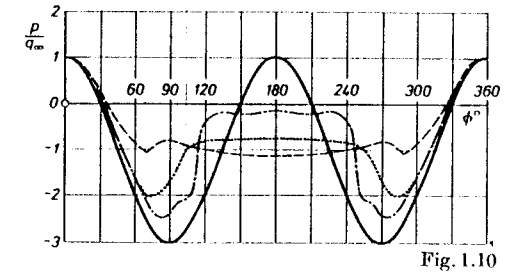


Fig. 1.10. Pressure distribution on a circular cylinder in the subcritical and supercritical range of Reynolds numbers after the measurements of O. Flachsbart [4] and A. Roshko [13].  $q_\infty = \frac{1}{2} \rho V^2$  is the stagnation pressure of the oncoming flows

— frictionless flow  
 - - -  $R = 1.9 \times 10^5$  Flachsbart (1932)  
 . . . .  $R = 6.7 \times 10^5$  Roshko (1961)  
 . . . .  $R = 8.4 \times 10^6$  Roshko (1961)

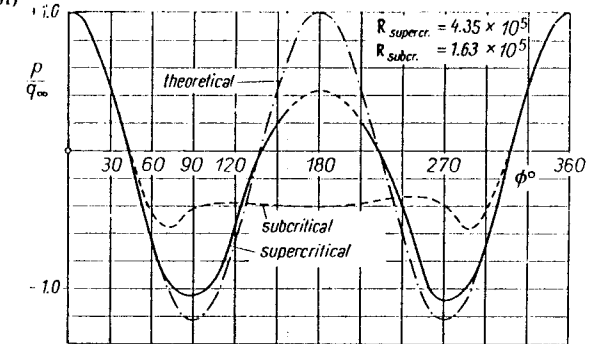


Fig. 1.11. Pressure distribution around a sphere in the subcritical and supercritical range of Reynolds numbers, as measured by O. Flachsbart [3]

of large drag coefficients, whereas the larger value lies in the range of small drag coefficients, Fig. 1.5. In this case the measured pressure-distribution curve for the large Reynolds number approximates the theoretical curve of frictionless flow very well over the greatest part of the circumference.

Considerably better agreement between the theoretical and measured pressure distribution is obtained for a streamline body in a flow parallel to its axis [5], Fig. 1.12. Good agreement exists here over almost the whole length of the body, with the exception of a small region near its trailing end. As will be shown later this circumstance is a consequence of the gradual pressure increase in the downstream direction.

Although, generally speaking, the theory of perfect fluids does not lead to useful results as far as drag calculations are concerned, the lift can be calculated from it very successfully. Fig. 1.13 represents the relation between the lift coefficient and angle of incidence, as measured by A. Betz [2] in the case of a Zhukovskii aerofoil

of infinite span and provides a comparison with theory. In the range of incidence angles  $\alpha = -10^\circ$  to  $10^\circ$  the agreement is seen to be good and the small differences can be explained by the influence of friction. The measured and calculated pressure distributions agree very well too, as shown in Fig. 1.14. The discrepancy between theory and measurement displayed in Figs. 1.13 and 1.14 is a consequence of the displacement action of the boundary layer and constitutes a boundary-layer effect of higher order, as will be shown again in Sec. IXj.

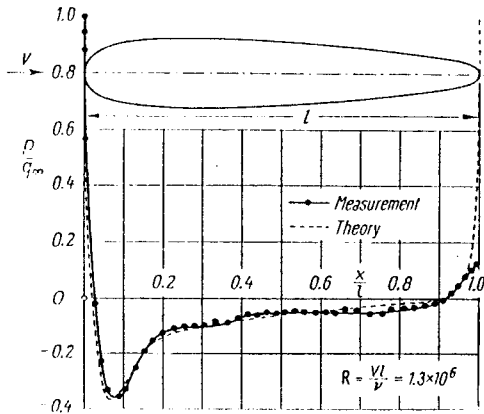


Fig. 1.12. Pressure distribution about a stream-line body of revolution; comparison between theory and measurement, after Fuhrmann [5]

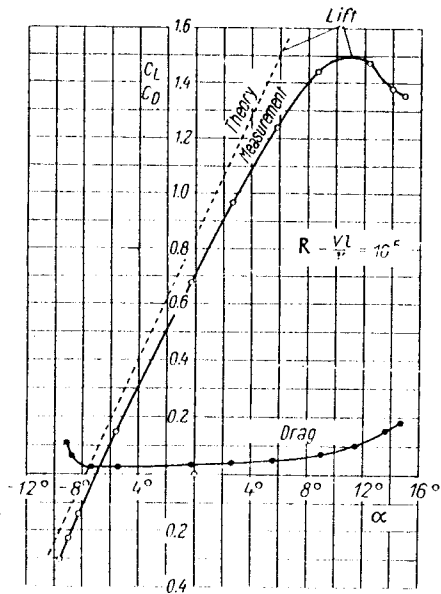
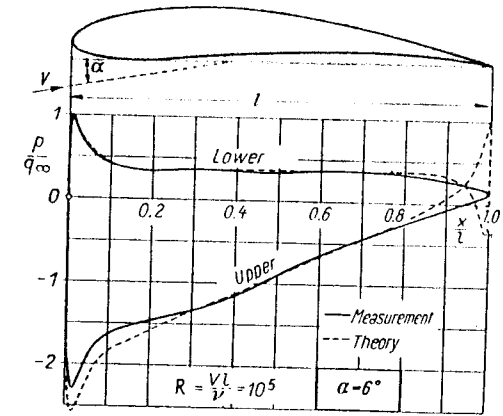


Fig. 1.13. Lift and drag coefficient of a Zhukovskii profile in plane flow, as measured by Betz [2]

Fig. 1.14. Comparison between the theoretical and measured pressure distribution for a Zhukovskii profile at equal lifts, after A. Betz [2]



References

- [1] Achenbach, E.: Experiments on the flow past spheres at very high Reynolds numbers. *JFM* 54, 565–575 (1972).
- [1a] Bailey, A. B., and Hiatt, J.: Sphere drag coefficients for a broad range of Mach and Reynolds numbers. *AIAA J.* 10, 1436–1440 (1972).
- [1b] Bailey, A. B., and Starr, R. F.: Sphere drag at transonic speeds and high Reynolds numbers. *AIAA J.* 14, 1631 (1976).
- [2] Betz, A.: Untersuchung einer Joukovskischen Tragfläche. *ZFM* 6, 173–179 (1915).
- [3] Flachsbar, O.: Neuere Untersuchungen über den Luftwiderstand von Kugeln. *Phys. Z.* 28, 461–469 (1927).
- [4] Flachsbar, O.: Winddruck auf Gasbehälter. Reports of the AVA in Göttingen. 1Vth Series, 134–138 (1932).
- [5] Fuhrmann, G.: Theoretische und experimentelle Untersuchungen an Ballonmodellen. Diss. Göttingen 1910; *Jb. Motorluftschiff-Studienges.* V 63–123 (1911/12).
- [6] Hagen, G.: Über die Bewegung des Wassers in engen zylindrischen Röhren. *Pogg. Ann.* 46, 423–442 (1839).
- [7] Homann, F.: Einfluss grosser Zähigkeit bei Strömung um Zylinder. *Forsch. Ing.-Wes.* 7, 1–10 (1936).
- [8] Jones, G. W., Cinotta, J. J., and Walker, R. W.: Aerodynamic forces on a stationary and oscillating circular cylinder at high Reynolds numbers. *NACA TR R-300* (1969).
- [9] Naumann, A.: Luftwiderstand von Kugeln bei hohen Unterschallgeschwindigkeiten. *Allgem. Wärmetechnik* 4, 217–221 (1953).
- [10] Naumann, A., and Pfeiffer, H.: Über die Grenzschichtströmung am Zylinder bei hohen Geschwindigkeiten. *Advances in Aeronautical Sciences* (Th. von Kármán, ed.) Vol. 3, 185–206, London, 1962.
- [11] Poiseuille, J.: Recherches expérimentelles sur le mouvement des liquides dans les tubes de très petits diamètres. *Comptes Rendus* 11, 961–967 and 1041–1048 (1840); 12, 112–115 (1841); in more detail: *Mémoires des Savants Etrangers* 9 (1846).
- [12] Reynolds, O.: An experimental investigation of the circumstances which determine whether the motion of water shall be direct or sinuous, and of the law of resistance in parallel channels. *Phil. Trans. Roy. Soc.* 174, 935–982 (1883) or *Scientific Papers* II, 51.
- [13] Roshko, A.: Experiments on the flow past a circular cylinder at very high Reynolds numbers. *JFM* 10, 345–356 (1961); see also: On the aerodynamic drag of cylinders at high Reynolds numbers. Paper presented at the US Japan Research Seminar on Wind Loads on Structures, Univ. of Hawaii, Oct. 1970.
- [14] Taneda, S.: Experimental investigation of the wakes behind cylinders and plates at low Reynolds numbers. *J. Phys. Soc. Japan* 11, 302–307 (1956).

## CHAPTER II

## Outline of boundary-layer theory

## a. The boundary-layer concept

In the case of fluid motions for which the measured pressure distribution nearly agrees with the perfect-fluid theory, such as the flow past the streamline body in Fig. 1.12, or the aerofoil in Fig. 1.14, the influence of viscosity at high Reynolds numbers is confined to a very thin layer in the immediate neighbourhood of the solid wall. If the condition of no slip were not to be satisfied in the case of a real fluid there would be no appreciable difference between the field of flow of the real fluid as compared with that of a perfect fluid. The fact that at the wall the fluid adheres to it means, however, that frictional forces retard the motion of the fluid in a thin layer near the wall. In that thin layer the velocity of the fluid increases from zero at the wall (no slip) to its full value which corresponds to external frictionless flow. The layer under consideration is called the *boundary layer*, and the concept is due to L. Prandtl [25].

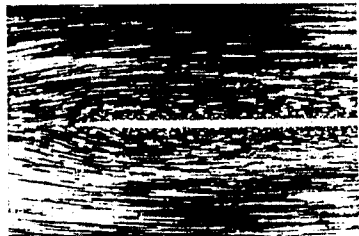


Fig. 2.1. Motion along a thin flat plate, from Prandtl-Tietjens

$l$  = length of plate;  
Reynolds number  $R = lU/\nu = 3$

Figure 2.1 reproduces a picture of the motion of water along a thin flat plate in which the streamlines were made visible by the sprinkling of particles on the surface of the water. The traces left by the particles are proportional to the velocity of flow. It is seen that there is a very thin layer near the wall in which the velocity is considerably smaller than at a larger distance from it. The thickness of this boundary layer increases along the plate in a downstream direction. Fig. 2.2 represents diagrammatically the velocity distribution in such a boundary layer at the

plate, with the dimensions across it considerably exaggerated. In front of the leading edge of the plate the velocity distribution is uniform. With increasing distance from the leading edge in the downstream direction the thickness,  $\delta$ , of the retarded layer increases continuously, as increasing quantities of fluid become affected. Evidently the thickness of the boundary layer decreases with decreasing viscosity.

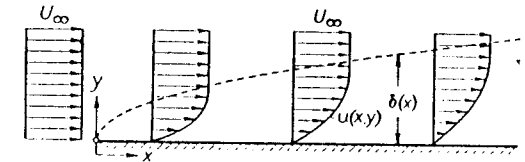


Fig. 2.2. Sketch of boundary layer on a flat plate in parallel flow at zero incidence

On the other hand, even with very small viscosities (large Reynolds numbers) the frictional shearing stresses  $\tau = \mu \partial u / \partial y$  in the boundary layer are considerable because of the large velocity gradient across the flow, whereas outside the boundary layer they are very small. This physical picture suggests that the field of flow in the case of fluids of small viscosity can be divided, for the purpose of mathematical analysis, into two regions: the thin boundary layer near the wall, in which friction must be taken into account, and the region outside the boundary layer, where the forces due to friction are small and may be neglected, and where, therefore, the perfect-fluid theory offers a very good approximation. Such a division of the field of flow, as we shall see in more detail later, brings about a considerable simplification of the mathematical theory of the motion of fluids of low viscosity. In fact, the theoretical study of such motions was only made possible by Prandtl when he introduced this concept.

We now propose to explain the basic concepts of boundary-layer theory with the aid of purely physical ideas and without the use of mathematics. The mathematical boundary-layer theory which forms the main topic of this book will be discussed in the following chapters.

The decelerated fluid particles in the boundary layer do not, in all cases, remain in the thin layer which adheres to the body along the whole wetted length of the wall. In some cases the boundary layer increases its thickness considerably in the downstream direction and the flow in the boundary layer becomes reversed. This causes the decelerated fluid particles to be forced outwards, which means that the boundary layer is separated from the wall. We then speak of *boundary-layer separation*. This phenomenon is always associated with the formation of vortices and with large energy losses in the wake of the body. It occurs primarily near blunt bodies, such as circular cylinders and spheres. Behind such a body there exists a region of strongly decelerated flow (so-called wake), in which the pressure distribution deviates considerably from that in a frictionless fluid, as seen from Figs. 1.10 and 1.11 in the respective cases of a cylinder and a sphere. The large drag of such bodies can be explained by the existence of this large deviation in pressure distribution, which is, in turn, a consequence of boundary-layer separation.

**Estimation of boundary-layer thickness:** The thickness of a boundary layer which has not separated can be easily estimated in the following way. Whereas friction forces can be neglected with respect to inertia forces outside the boundary layer, owing to low viscosity, they are of a comparable order of magnitude inside it. The inertia force per unit volume is, as explained in Section I e, equal to  $\rho u \partial u / \partial x$ . For a plate of length  $l$  the gradient  $\partial u / \partial x$  is proportional to  $U/l$ , where  $U$  denotes the velocity outside the boundary layer. Hence the inertia force is of the order  $\rho U^2/l$ . On the other hand the friction force per unit volume is equal to  $\partial \tau / \partial y$ , which, on the assumption of laminar flow, is equal to  $\mu \partial^2 u / \partial y^2$ . The velocity gradient  $\partial u / \partial y$  in a direction perpendicular to the wall is of the order  $U/\delta$  so that the friction force per unit volume is  $\partial \tau / \partial y \sim \mu U / \delta^2$ . From the condition of equality of the friction and inertia forces the following relation is obtained:

$$\mu \frac{U}{\delta^2} \sim \frac{\rho U^2}{l}$$

or, solving for the boundary-layer thickness  $\delta$  †:

$$\delta \sim \sqrt{\frac{\mu l}{\rho U}} = \sqrt{\frac{\nu l}{U}}. \quad (2.1)$$

The numerical factor which is, so far, still undetermined will be deduced later (Chap. VII) from the exact solution given by H. Blasius [4], and it will turn out that it is equal to 5, approximately. Hence for *laminar* flow in the boundary layer we have

$$\delta = 5 \sqrt{\frac{\nu l}{U}}. \quad (2.1a)$$

The dimensionless boundary-layer thickness, referred to the length of the plate,  $l$ , becomes:

$$\frac{\delta}{l} = 5 \sqrt{\frac{\nu}{U l}} = \frac{5}{\sqrt{R_l}}, \quad (2.2)$$

where  $R_l$  denotes the Reynolds number related to the length of the plate,  $l$ . It is seen from eqn. (2.1) that the boundary-layer thickness is proportional to  $\sqrt{\nu}$  and to  $\sqrt{l}$ . If  $l$  is replaced by the variable distance  $x$  from the leading edge of the plate, it is seen that  $\delta$  increases proportionately to  $\sqrt{x}$ . On the other hand the relative boundary-layer thickness  $\delta/l$  decreases with increasing Reynolds number as  $1/\sqrt{R}$  so that in the limiting case of frictionless flow, with  $R \rightarrow \infty$ , the boundary-layer thickness vanishes.

We are now in a position to estimate the shearing stress  $\tau_0$  on the wall, and consequently, the total drag. According to Newton's law of friction (1.2) we have

$$\tau_0 = \mu \left( \frac{\partial u}{\partial y} \right)_0,$$

† A more rigorous definition of boundary-layer thickness is given at the end of this section.

where subscript 0 denotes the value at the wall, i. e. for  $y = 0$ . With the estimate  $(\partial u / \partial y)_0 \sim U/\delta$  we obtain  $\tau_0 \sim \mu U/\delta$  and, inserting the value of  $\delta$  from eqn. (2.1), we have

$$\tau_0 \sim \mu U \sqrt{\frac{\rho U}{\mu l}} = \sqrt{\frac{\mu \rho U^3}{l}}. \quad (2.3)$$

Thus the frictional stress near the wall is proportional to  $U^{3/2}$ .

We can now form a dimensionless stress with reference to  $\rho U^2$ , as explained in Chap. I, and obtain

$$\frac{\tau_0}{\rho U^2} \sim \sqrt{\frac{\mu}{\rho U l}} = \frac{1}{\sqrt{R_l}}. \quad (2.3a)$$

This result agrees with the dimensional analysis in Chap. I, which predicted that the dimensionless shearing stress could depend on the Reynolds number only.

The total drag  $D$  on the plate is equal to  $bl\tau_0$  where  $b$  denotes the width of the plate. Hence, with the aid of eqn. (2.3) we obtain

$$D \sim b \sqrt{\frac{\mu \rho U^3 l}{l}}. \quad (2.4)$$

The laminar frictional drag is thus seen to be proportional to  $l^{3/2}$  and  $l^{1/2}$ . Proportionality to  $l^{1/2}$  means that doubling the plate length does not double the drag, and this result can be understood by considering that the downstream part of the plate experiences a smaller drag than the leading portion because the boundary layer is thicker towards the trailing edge. Finally, we can write down an expression for the dimensionless drag coefficient in accordance with eqn. (1.14) in which the reference area  $A$  will be replaced by the wetted area  $bl$ . Hence eqn. (2.4) gives that

$$C_D \sim \sqrt{\frac{\mu}{\rho U l}} = \frac{1}{\sqrt{R_l}}.$$

The numerical factor follows from H. Blasius's exact solution, and is 1.328, so that the drag of a plate in parallel laminar flow becomes

$$C_D = \frac{1.328}{\sqrt{R_l}}. \quad (2.5)$$

The following numerical example will serve to illustrate the preceding estimation: Laminar flow, stipulated here, is obtained, as is known from experiment, for Reynolds numbers  $Ul/\nu$  not exceeding about  $5 \times 10^5$  to  $10^6$ . For larger Reynolds numbers the boundary layer becomes turbulent. We shall now calculate the boundary-layer thickness for the flow of air ( $\nu = 0.144 \times 10^{-3}$  ft<sup>2</sup>/sec) at the end of a plate of length  $l = 3$  ft at a velocity  $U = 48$  ft/sec. This gives  $R_l = Ul/\nu = 10^6$  and from eqn. (2.2)

$$\frac{\delta}{l} = \frac{5}{10^3} = 0.005; \quad \delta = 0.18 \text{ in.}$$

The drag coefficient from eqn. (2.5) is  $C_D = 0.0013$  i. e. exceedingly small when compared with that for a circular cylinder, Fig. 1.4, because the drag coefficient for a cylinder also includes pressure forces.

**Definition of boundary-layer thickness:** The definition of the boundary-layer thickness is to a certain extent arbitrary because transition from the velocity in the boundary to that outside it takes place asymptotically. This is, however, of no practical importance, because the velocity in the boundary layer attains a value which is very close to the external velocity already at a small distance from the wall. It is possible to define the boundary-layer thickness as that distance from the wall where the velocity differs by 1 per cent from the external velocity. With this definition the numerical factor in eqn. (2.2) has the value 5. Instead of the boundary-layer thickness, another quantity, the *displacement thickness*  $\delta_1$ , is sometimes used, Fig. 2.3. It is defined by the equation

$$U \delta_1 = \int_0^{\infty} (U - u) dy. \quad (2.6)$$

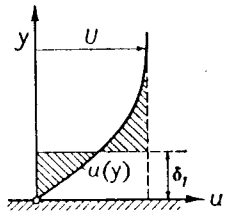


Fig. 2.3. Displacement thickness  $\delta_1$  in a boundary layer

The displacement thickness indicates the distance by which the external streamlines are shifted owing to the formation of the boundary layer. In the case of a plate in parallel flow and at zero incidence the displacement thickness is about  $\frac{1}{3}$  of the boundary-layer thickness  $\delta$  given in eqn. (2.1 a).

### b. Separation and vortex formation

The boundary layer near a flat plate in parallel flow and at zero incidence is particularly simple, because the static pressure remains constant in the whole field of flow. Since outside the boundary layer the velocity remains constant the same applies to the pressure because in the frictionless flow Bernoulli's equation remains valid. Furthermore, the pressure remains sensibly constant over the width of the boundary layer at a given distance  $x$ . Hence the pressure over the width of the boundary layer has the same magnitude as outside the boundary layer at the same distance, and the same applies to cases of arbitrary body shapes when the pressure outside the boundary layer varies along the wall with the length of arc. This fact is expressed by saying that the external pressure is "impressed" on the boundary layer. Hence in the case of the motion past a plate the pressure remains constant throughout the boundary layer.

The phenomenon of boundary-layer separation mentioned previously is intimately connected with the pressure distribution in the boundary layer. In the boundary layer on a plate no separation takes place as no back-flow occurs.

In order to explain the very important phenomenon of boundary-layer separation let us consider the flow about a blunt body, e. g. about a circular cylinder, as shown in Fig. 2.4. In frictionless flow, the fluid particles are accelerated on the upstream

half from  $D$  to  $E$ , and decelerated on the downstream half from  $E$  to  $F$ . Hence the pressure decreases from  $D$  to  $E$  and increases from  $E$  to  $F$ . When the flow is started up the motion in the first instant is very nearly frictionless, and remains so as long as the boundary layer remains thin. Outside the boundary layer there is a transformation of pressure into kinetic energy along  $D E$ , the reverse taking place along  $E F$ , so that a particle arrives at  $F$  with the same velocity as it had at  $D$ . A fluid particle which moves in the immediate vicinity of the wall in the boundary layer remains under the influence of the same pressure field as that existing outside, because the external pressure is impressed on the boundary layer. Owing to the large friction forces in the thin boundary layer such a particle consumes so much of its kinetic

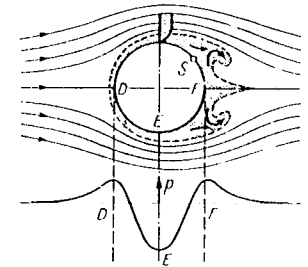


Fig. 2.4. Boundary-layer separation and vortex formation on a circular cylinder (diagrammatic)  $S$  = point of separation

energy on its path from  $D$  to  $E$  that the remainder is too small to surmount the "pressure hill" from  $E$  to  $F$ . Such a particle cannot move far into the region of increasing pressure between  $E$  and  $F$  and its motion is, eventually, arrested. The external pressure causes it then to move in the opposite direction. The photographs reproduced in Fig. 2.5 illustrate the sequence of events near the downstream side of a round body when a fluid flow is started. The pressure increases along the body contour from left to right, the flow having been made visible by sprinkling aluminium dust on the surface of the water. The boundary layer can be easily recognized by reference to the short traces. In Fig. 2.5 a, taken shortly after the start of the motion, the reverse motion has just begun. In Fig. 2.5 b the reverse motion has penetrated a considerable distance forward and the boundary layer has thickened appreciably. Fig. 2.5 c shows how this reverse motion gives rise to a vortex, whose size is increased still further in Fig. 2.5 d. The vortex becomes separated shortly afterwards and moves downstream in the fluid. This circumstance changes completely the field of flow in the wake, and the pressure distribution suffers a radical change, as compared with frictionless flow. The final state of motion can be inferred from Fig. 2.6. In the eddying region behind the cylinder there is considerable suction, as seen from the pressure distribution curve in Fig. 1.10. This suction causes a large pressure drag on the body.

At a larger distance from the body it is possible to discern a regular pattern of vortices which move alternately clockwise and counterclockwise, and which is known as a Kármán vortex street [20], Fig. 2.7 (see also Fig. 1.6). In Fig. 2.6 a vortex moving in a clockwise direction can be seen to be about to detach itself from the body before joining the pattern. In a further paper, von Kármán [21] proved that such vortices are generally unstable with respect to small disturbances parallel

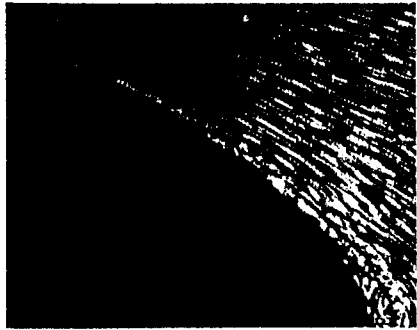


Fig. 2.5a

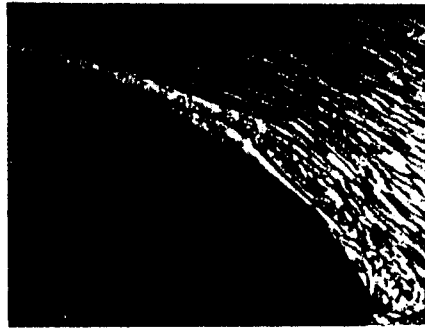


Fig. 2.5b

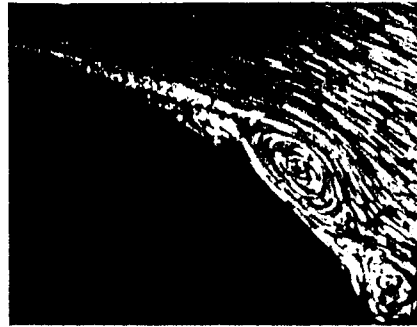


Fig. 2.5c

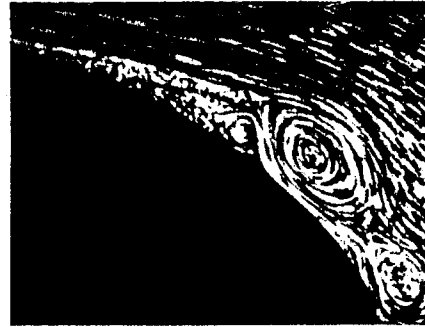


Fig. 2.5d

Fig. 2.5a, b, c, d. Development of boundary-layer separation with time, after Prandtl-Tietjens [27]. See also Fig. 15.5

to themselves. The only arrangement which shows neutral equilibrium is that with  $h/l = 0.281$  (Fig. 2.8). The vortex street moves with a velocity  $u$ , which is smaller than the flow velocity  $U$  in front of the body. It can be regarded as a highly idealized picture of the motion in the wake of the body. The kinetic energy contained in the velocity field of the vortex street must be continually created, as the body moves through the fluid. On the basis of this representation it is possible to deduce an expression for the drag from the perfect-fluid theory. Its magnitude per unit length of the cylindrical body is given by

$$D = \rho U^2 h \left[ 2.83 \frac{u}{U} - 1.12 \left( \frac{u}{U} \right)^2 \right].$$

The width  $h$ , and the velocity ratio  $u/U$  must be known from experiment.

More recent experimental investigations due to W. W. Durgin and others [13] established that in an accelerating vortex street the ratio of the longitudinal to the transverse spacing of the vortices changes considerably. As a result, the regular arrangement of vortices is transformed into a turbulent wake.

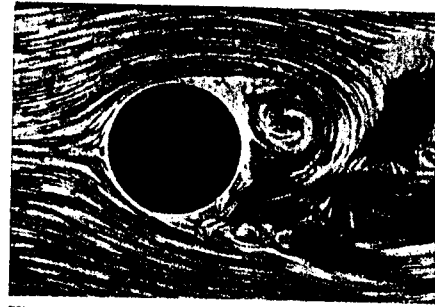


Fig. 2.6

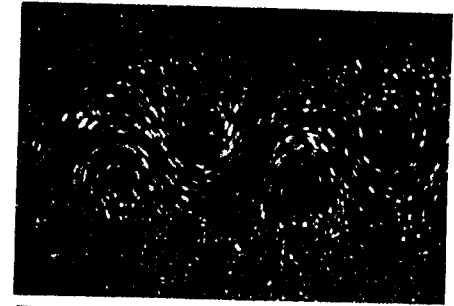


Fig. 2.7

Fig. 2.6. Instantaneous photograph of flow with complete boundary-layer separation in the wake of a circular cylinder, after Prandtl-Tietjens [27]

Fig. 2.7. Kármán vortex street, from A. Timme [38]

Fig. 2.8. Streamlines in a vortex street ( $h/l = 0.28$ ). The fluid is at rest at infinity, and the vortex street moves to the left.

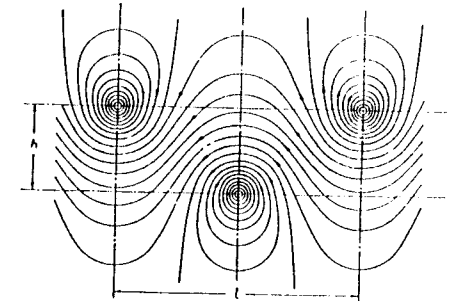


Fig. 2.8

**Circular cylinder.** The frequency with which vortices are shed in a Kármán vortex street behind a circular cylinder was first extensively measured by H. Blenk, D. Fuchs and L. Liebers [5]. A regular Kármán street is observed only in the range of Reynolds numbers  $VD/\nu$  from about 60 to 5000. At lower Reynolds numbers the wake is laminar and has the form visible in the first two photographs of Fig. 1.6; at higher Reynolds numbers there is complete turbulent mixing. Measurements show that in the regular range given above, the dimensionless frequency,

$$\frac{nD}{V} = S, \quad (\text{Strouhal number})$$

also known as the Strouhal number [37], depends only on the Reynolds number. This relationship is shown plotted in Fig. 2.9 which is based on measurements performed by A. Roshko [32]; see also [15]. The experimental points which were obtained with cylinders of different diameters  $D$  and at different velocities  $V$  arrange themselves well on a single curve. At the higher Reynolds numbers the Strouhal number remains approximately constant at  $S = 0.21$ . This value of  $S$ , as seen from Fig. 2.9, prevails up to a Reynolds number  $R = 2 \times 10^5$ , that is in the subcritical range (see also Fig. 1.4). At higher Reynolds numbers, say around  $R = 10^6$ , a regular vortex street does not exist. According to A. Roshko [31], such a regular street re-appears at extremely large Reynolds numbers ( $R > 3 \times 10^6$ ) when the Strouhal

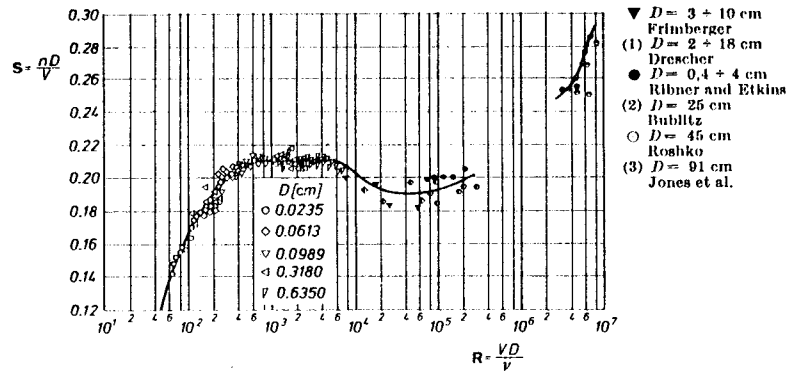


Fig. 2.9. The Strouhal number,  $S$ , for the Kármán vortex street in the flow past a circular cylinder in terms of the Reynolds number,  $R$ . Measurements performed by A. Roshko [31, 32], H. S. Ribner, B. Etkins and K. K. Nelly [30], E. F. Relf and L. F. G. Simmons [28] as well as G. W. Jones et al. ([8] of Chap. I). In the range  $R = 3 \times 10^5$  to  $3 \times 10^6$  (supercritical regime with very low drag. Fig 1.4) the Kármán vortex street is no longer regular. It is only at  $R > 4 \times 10^6$  that a regular pattern forms again; its Strouhal number is now higher at  $S = 0.26$  to  $0.30$  compared with  $S \approx 0.20$  at  $R = 10^3$  to  $3 \times 10^5$

number assumes values around  $S = 0.27$ . In this connexion the paper by P.W. Bearman [3a] may also be consulted. When the diameters of the cylinders are small and the velocities are moderate, the resulting frequencies lie in the acoustic range. For example, the familiar "aeolian tones" emitted by telegraph wires are the result of these phenomena. At a velocity of  $V = 10$  m/sec (30.48 ft/sec) and a wire of 2 mm (0.079 in) in diameter, the frequency becomes  $n = 0.21$  ( $10/0.002$ ) =  $1050 \text{ sec}^{-1}$ , and the corresponding Reynolds number  $R \approx 1200$ .

**Flat plate at zero incidence.** The fact that a regular vortex street establishes itself, among others, behind slender bodies as well as in compressible streams has only been established recently by H. J. Heinemann et al. [18]. The photograph of Fig. 2.10 shows such a regular vortex street behind a flat plate at zero incidence for a Mach number  $M_\infty = 0.61$ . The diagram in Fig. 2.11 contains a plot of the Strouhal number,  $S = nd/V$ , formed with the plate thickness,  $d$ , in terms of the Mach number, but only for the subsonic range  $M = 0.2$  to  $0.85$ . The diagram proves that here too  $S \approx 0.2$ , as was the case for the circular cylinder in Fig. 2.9. The corresponding Reynolds numbers, referred to the length of the plate, are in the range  $R = Vl/v = 3 \times 10^5$  to  $8 \times 10^5$  in which the flow is laminar.

Two papers by C. C. Lin. [22] and U. Domm [11] concern themselves with the theory of the Kármán vortex street. The formation of a vortex pair behind a flat plate in cross-flow at right angles to it has been investigated theoretically by E. Wedemeyer [38a], whereas T. Sarpkaya [33b] conducted theoretical and experimental studies for a plate arranged at a large angle of attack (see Fig. 4.2); in this connexion

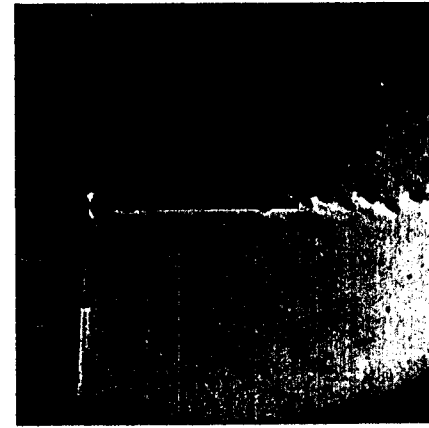


Fig. 2.10. Von Kármán vortex street behind a flat plate at zero incidence at a Mach number  $M = 0.61$  and a Reynolds number  $R = Vl/v = 6.5 \times 10^5$  after H. J. Heinemann et al. [18]. Length of plate  $l = 60$  mm, thickness ratio  $d/l = 0.05$ . Exposure time approx. 20 nanosec ( $20 \times 10^{-9}$  sec)

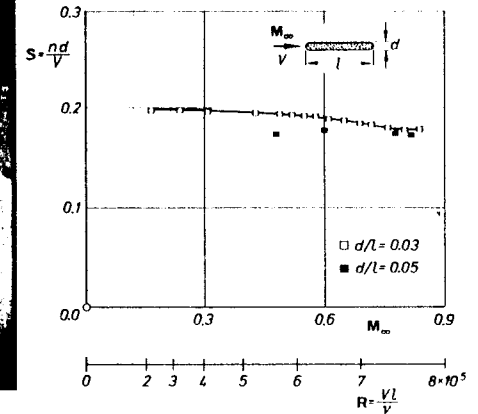


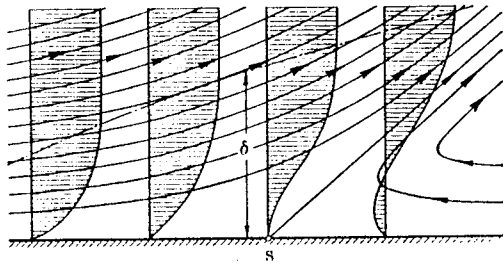
Fig. 2.11. Strouhal number  $S = nd/V$  in terms of the Mach number for the vortex street behind a flat plate at zero incidence, after H. J. Heinemann et al. [18]

an earlier paper by L. Rosenhead [32a] may also be consulted. The reader may also be interested to look up the text of a remark made by L. Prandtl on the occasion of a lecture by K. Friedrichs („Bemerkung über die ideale Strömung um einen Körper bei verschwindender Zähigkeit“ Lectures on aerodynamics and allied subjects, Aachen 1929, Springer, Berlin 1930, pp. 51, 52).

**Separation.** The boundary-layer theory succeeds in this manner, i.e. with the aid of the explanation of the phenomenon of separation; in throwing light on the occurrence of pressure or form drag in addition to viscous drag. The danger of boundary-layer separation exists always in regions with an adverse pressure gradient and the likelihood of its occurrence increases in the case of steep pressure curves, i.e. behind bodies with blunt ends. The preceding argument explains also why the experimental pressure distribution shown in Fig. 1.11 for the case of a slender streamline body differs so little from that predicted for frictionless flow. The pressure increase in the downstream direction is here so gradual, that there is no separation. Consequently, there is no appreciable pressure drag and the total drag consists mainly of viscous drag and is, therefore, small.

The streamlines in the boundary layer near separation are shown diagrammatically in Fig. 2.12. Owing to the reversal of the flow there is a considerable thickening of the boundary layer, and associated with it, there is a flow of boundary-layer material into the outside region. At the point of separation one streamline inter-





$S$  = point of separation

Fig. 2.12. Diagrammatic representation of flow in the boundary layer near a point of separation

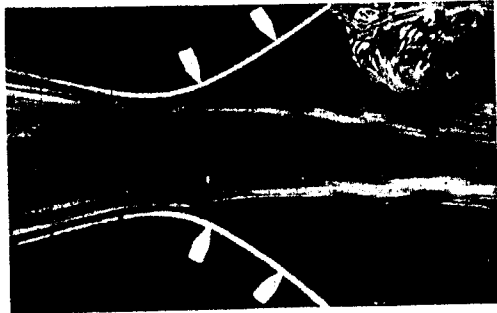


Fig. 2.13. Flow with separation in a highly divergent channel, from Prandtl-Tietjens [27]

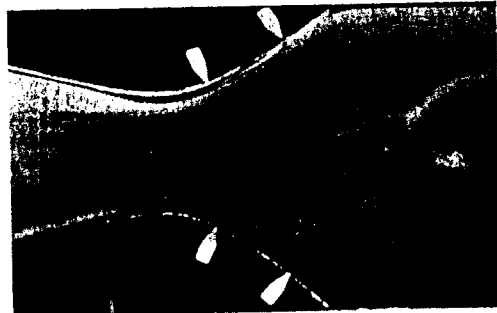


Fig. 2.14. Flow with boundary-layer suction on upper wall of highly divergent channel

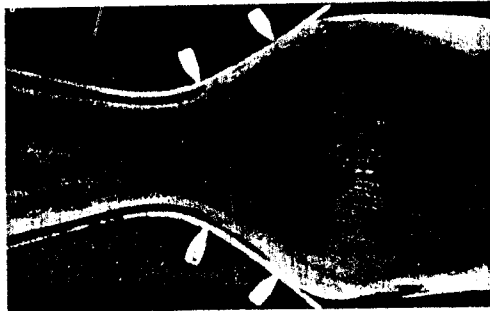


Fig. 2.15. Flow with boundary-layer suction on both walls of highly divergent channel

sects the wall at a definite angle, and the point of separation itself is determined by the condition that the velocity gradient normal to the wall vanishes there:

$$\left(\frac{\partial u}{\partial y}\right)_{wall} = 0 \quad (\text{separation}). \quad (2.7)$$

The precise location of the point of separation can be determined only with the aid of an exact calculation, i. e. by the integration of the boundary-layer equations.

Separation, as described for the case of a circular cylinder, can also occur in a highly divergent channel, Fig. 2.13. In front of the throat the pressure decreases in the direction of flow, and the flow adheres completely to the walls, as in a frictionless fluid. However, behind the throat the divergence of the channel is so large that the boundary layer becomes separated from both walls, and vortices are formed. The stream fills now only a small portion of the cross-sectional area of the channel. However, separation is prevented if boundary-layer suction is applied at the wall (Figs. 2.14 and 2.15).

The photographs in Figs. 2.16 and 2.17† prove that the adverse pressure gradient together with friction near the wall determine the process of separation which is independent of such other circumstance as e. g. the curvature of the wall. The first picture shows the motion of a fluid against a wall at right angles to it (plane stagnation flow). Along the streamline in the plane of symmetry which leads to the stagnation point there is a considerable pressure increase in the direction of flow. No separation, however, occurs, because no wall friction is present. There is no separation near the wall, either, because here the flow in the boundary layer takes place in the direction of decreasing pressure on both sides of the plane of symmetry. If now a thin wall is placed along the plane of symmetry at right angles to the first wall, Fig. 2.17, the new boundary layer will show a pressure increase in the direction of flow. Consequently, separation now occurs near the plane wall. The incidence of separation is often rather sensitive to small changes in the shape of the solid body, particularly when the pressure distribution is strongly affected by this change in shape. A very instructive example is given in the pictures of Fig. 2.18 which show photographs of the flow field about a model of a motor vehicle (the Volkswagen delivery van), [23, 35]. When the nose was flat giving it an angular shape (a), the flow past the fairly sharp corners in front caused large suction followed by a large pressure increase along the side walls. This led to complete separation and to the formation of a wide wake behind the body. The drag coefficient of the vehicle with this angular shape had a value of  $C_D = 0.76$ . The large suction near the front end and the separation along the side walls were eliminated when the shape was changed by adding the round nose shown at (b). Simultaneously, the drag coefficient became markedly smaller and had a value of  $C_D = 0.42$ . Further research on such vehicles has been performed by W. H. Hucho [19] for the case of a non-symmetric stream.

† Fig. 2.16. and 2.17. have been taken from the paper "Strömungen in Dampfkesselanlagen" by H. Foettinger, Mitteilungen der Vereinigung ~~der~~ Kesselbesitzer, No. 73, p. 151 (1939).

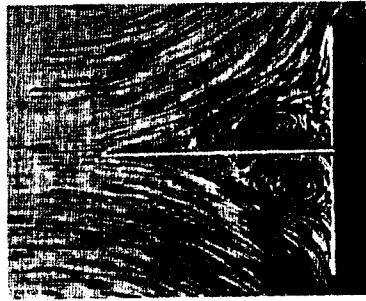
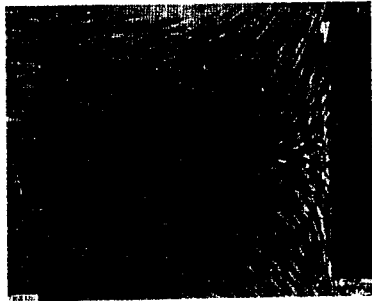


Fig. 2.16. Free stagnation flow without separation, as photographed by Foettinger

Fig. 2.17. Decelerated stagnation flow with separation, as photographed by Foettinger


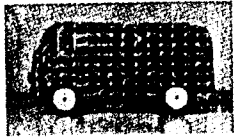
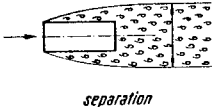
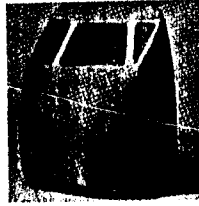
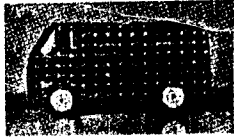
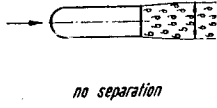
<p>(a) Angular nose</p>    <p style="text-align: center;">separation</p>		$C_D =$  0.76
<p>(b) Round nose</p>    <p style="text-align: center;">no separation</p>		  0.42

Fig. 2.18. Flow about a model of a motor vehicle (Volkswagen delivery van), after E. Moeller [23]. a) Angular nose with separated flow along the whole of the side wall and large drag coefficient ( $C_D = 0.76$ ); b) Round nose with no separation and small drag coefficient ( $C_D = 0.42$ )

Separation is also important for the lifting properties of an aerofoil. At small incidence angles (up to about  $10^\circ$ ) the flow does not separate on either side and closely approximates frictionless conditions. The pressure distribution for such a case ("sound" flow, Fig. 2.19a) was given in Fig. 1.14. With increasing incidence there is danger of separation on the suction side of the aerofoil, because the pressure increase becomes steeper. For a given angle of incidence, which is about  $15^\circ$ , separation finally occurs. The separation point is located fairly closely behind the leading edge. The wake, Fig. 2.19b, shows a large "dead-water" area. The frictionless, lift-creating flow pattern has become disturbed, and the drag has become very large. The beginning of separation nearly coincides with the occurrence of maximum lift of the aerofoil.

**Structural aerodynamics.** Flow around land-based bluff bodies, such as structures and buildings, is considerably more complex than flow around streamlined bodies and aircraft. The principal cause of complication is the presence of the ground and the shear created in the turbulent wind as a consequence. The interaction between the incident shear flow and the structure produces coexisting static and dynamic loads [8, 9, 10]. The fluctuating forces produced by vortex formation and shedding can induce oscillations in the structures at their natural frequencies.

The flow patterns observed on a detached rectangular building is shown schematically in Fig. 2.20. In front of the building there appears a bound vortex which arises from the interaction of the boundary layer in the sheared flow ( $dV/dz > 0$ ) and the ground. There is, furthermore, strong vortex shedding from the sharp corners of the building and a complex wake is created behind it. So far no theoretical methods have been developed to cope with this extremely complicated flow pattern. It is, therefore, necessary to resort to wind-tunnel studies with the aid of adequately scaled models.

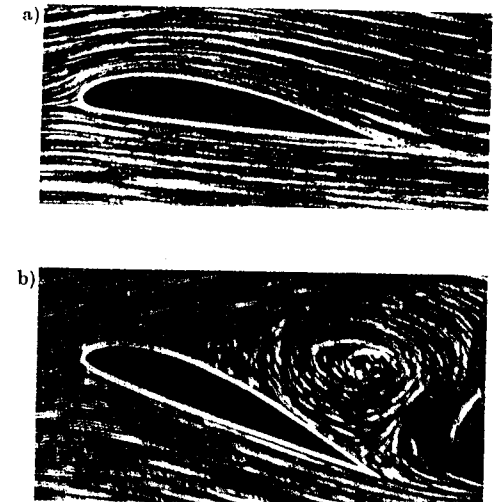


Fig. 2.19a.b. Flow around an aerofoil, after Prandtl-Tietjens [27]. a) 'sound' flow, b) flow with separation

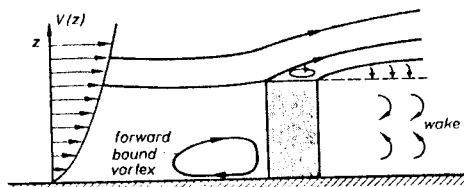


Fig. 2.20a

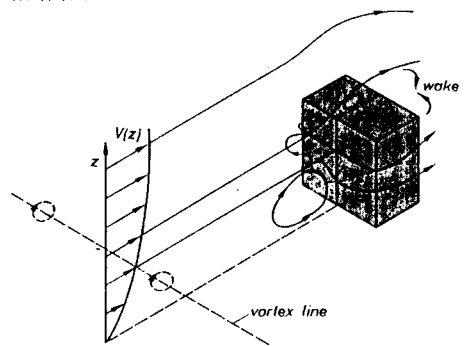


Fig. 2.20b

Fig. 2.20. Overall view of flow pattern (schematic) around a rectangular structure [34]. a) Side view with forward bound vortex in the stagnation zone and a separated roof boundary layer; b) upwind face and vortex shedding from the the windward corner of the roof

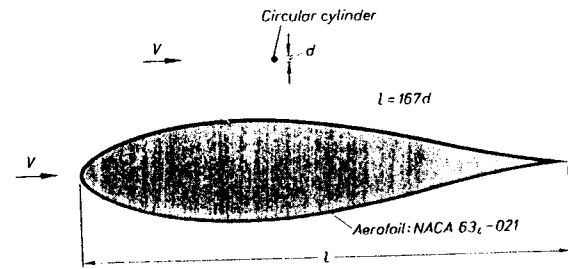


Fig. 2.22a

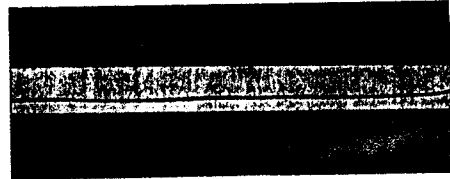


Fig. 2.22b



Fig. 2.21. Aerofoil and circular cylinder drawn in such relation to each other as to produce the same drag in parallel flows (parallel to axis of symmetry of aerofoil) of the same velocity. Aerofoil: Laminar aerofoil NACA 634-021 with laminar boundary layer. Drag coefficient  $c_{D0} = 0.006$  at  $R_r = 10^6$  to  $10^7$ , Fig. 17.14. Circular cylinder: Drag coefficient  $c_D = 1.0$  at  $R_d = 10^4$  to  $10^5$ ; Fig. 1.4. Thus the ratio of the chord of the aerofoil,  $l$ , to the diameter,  $d$ , of the cylinder is  $l/d = 1.0/0.006 = 167$

Fig. 2.22. The Reynolds dye experiment. Flow in water made visible by the injection of a dye, after W. Dubs [12]; a) laminar flow,  $R = 1150$ ; b) turbulent flow,  $R = 2520$

To conclude this section, we wish to discuss a particularly telling example of how effectively it is possible to reduce the drag of a body in a stream when the separation of the boundary layer is completely eliminated and when, in addition, the body itself is given a shape which is conducive to low resistance. Fig. 2.21 illustrates the effect of a favorable shape (streamline body) on drag: a symmetric aerofoil and a circular cylinder (thin wire) have been drawn here to a relative scale which assures equal drag in streams of equal velocity. The cylinder has a drag coefficient  $C_D \approx 1$  with respect to its frontal area (see also Fig. 1.4). On the other hand, the drag coefficient of the aerofoil, referred to its cross-sectional area, has the very low value of  $C_D = 0.006$ . The extremely low drag of the aerofoil is achieved as a result of a carefully chosen profile which assures that the boundary layer remains laminar over almost the whole of its wetted length (laminar aerofoil). In this connexion, Chap. XVII and, especially, Fig. 17.14, should be consulted.

c. Turbulent flow in a pipe and in a boundary layer

Measurements show that the type of motion through a circular pipe which was calculated in Section 1d, and in which the velocity distribution was parabolic, exists only at low and moderate Reynolds numbers. The fact that in the laminar motion under discussion fluid laminae slide over each other, and that there are no radial velocity components, so that the pressure drop is proportional to the first power of the mean flow velocity, constitutes an essential characteristic of this type of flow. This characteristic of the motion can be made clearly visible by introducing a dye into the stream and by discharging it through a thin tube, Fig. 2.22. At the moderate Reynolds numbers associated with laminar flow the dye is visible in the form of a clearly defined thread extending over the whole length of the pipe, Fig. 2.22a. By increasing the flow velocity it is possible to reach a stage when the fluid particles cease to move along straight lines and the regularity of the motion breaks down. The coloured thread becomes mixed with the fluid, its sharp outline becomes blurred and eventually the whole cross-section becomes coloured, Fig. 2.22b. On the axial motion there are now superimposed irregular radial fluctuations which effect the mixing. Such a flow pattern is called *turbulent*. The dye experiment was first carried out by O. Reynolds [29], who ascertained that the transition from the laminar to the turbulent type of motion takes place at a definite value of the Reynolds number (critical Reynolds number). The actual value of the critical Reynolds number depends further on the details of the experimental arrangement, in particular on the amount of disturbance suffered by the fluid before entering the pipe. With an arrangement which is as free from disturbances as possible critical Reynolds numbers  $(\bar{u}d/\nu)_{crit}$  exceeding  $10^4$  can be attained ( $\bar{u}$  = denotes the mean velocity averaged over the cross-sectional area). With a sharp-edged entrance the critical Reynolds number becomes approximately

$$\left(\frac{\bar{u} d}{\nu}\right)_{crit} = R_{crit} \approx 2300 \quad (\text{pipe}). \tag{2.8}$$

This value can be regarded as the lower limit for the critical Reynolds number below which even strong disturbances do not cause the flow to become turbulent.

In the turbulent region the pressure drop becomes approximately proportional to the square of the mean flow velocity. In this case a considerably larger pressure difference is required in order to pass a fixed quantity of fluid through the pipe, as compared with laminar flow. This follows from the fact that the phenomenon of turbulent mixing dissipates a large quantity of energy which causes the resistance to flow to increase considerably. Furthermore, in the case of turbulent flow the velocity distribution over the cross-sectional area is much more even than in laminar flow. This circumstance is also to be explained by turbulent mixing which causes an exchange of momentum between the layers near the axis of the tube and those near the walls. Most pipe flows which are encountered in engineering appliances occur at such high Reynolds numbers that turbulent motion prevails as a rule. The laws of turbulent motion through pipes will be discussed in detail in Chap. XX.

In a way which is similar to the motion through a pipe, the flow in a boundary layer along a wall also becomes turbulent when the external velocity is sufficiently large. Experimental investigations into the transition from laminar to turbulent flow in the boundary layer were first carried out by J. M. Burgers [6] and B. G. van der Hegge Zijnen [17] as well as by M. Hansen [16]. The transition from laminar to turbulent flow in the boundary layer becomes most clearly discernible by a sudden and large increase in the boundary-layer thickness and in the shearing stress near the wall. According to eqn. (2.1), with  $l$  replaced by the current co-ordinate  $x$ , the dimensionless boundary-layer thickness  $\delta/\sqrt{\nu x/U_\infty}$  becomes constant for laminar flow, and is, as seen from eqn. (2.1a), approximately equal to 5. Fig. 2.23 contains a plot of this dimensionless boundary-layer thickness against the Reynolds number  $U_\infty x/\nu$ . At  $R_x > 3.2 \times 10^5$  a very sharp increase is clearly visible, and

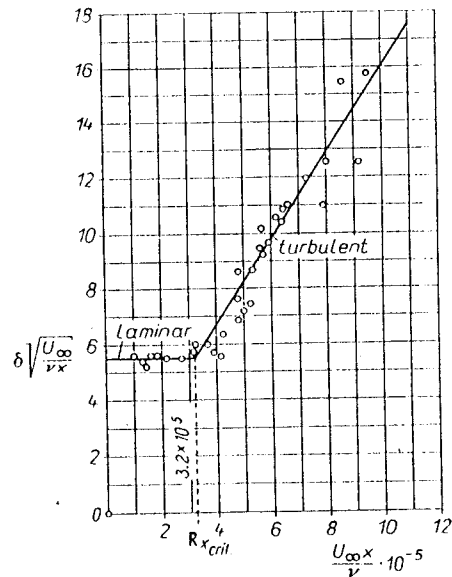


Fig. 2.23. Boundary-layer thickness plotted against the Reynolds number based on the current length  $x$  along a plate in parallel flow at zero incidence, as measured by Hansen [16]

an identical phenomenon is observed in a plot of wall shearing stress. The sudden increase in these quantities denotes that the flow has changed from laminar to turbulent. The Reynolds number  $R_x$  based on the current length  $x$  is related to the Reynolds number  $R_\delta = U_\infty \delta/\nu$  based on the boundary-layer thickness through the equation

$$R_\delta = 5 \sqrt{R_x}$$

as seen from eqn. (2.1a). Hence to the critical Reynolds number

$$R_{x \text{ crit}} = \left( \frac{U_\infty x}{\nu} \right)_{\text{crit}} = 3.2 \cdot 10^5 \quad (\text{plate})$$

there corresponds  $R_{\delta \text{ crit}} \approx 2800$ . The boundary layer on a plate is laminar near the leading edge and becomes turbulent further downstream. The abscissa  $x_{\text{crit}}$  of the point of transition can be determined from the known value of  $R_{x \text{ crit}}$ . In the case of a plate, as in the previously discussed pipe flow, the numerical value of  $R_{\text{crit}}$  depends to a marked degree on the amount of disturbance in the external flow, and the value  $R_{x \text{ crit}} = 3.2 \times 10^5$  should be regarded as a lower limit. With exceptionally disturbance-free external flow, values of  $R_{x \text{ crit}} = 10^6$  and higher have been attained.

A particularly remarkable phenomenon connected with the transition from laminar to turbulent flow occurs in the case of blunt bodies, such as circular cylinders or spheres. It will be seen from Figs. 1.4 and 1.5 that the drag coefficient of a circular cylinder or a sphere suffers a sudden and considerable decrease near Reynolds numbers  $V D/\nu$  of about  $5 \times 10^5$  or  $3 \times 10^5$  respectively. This fact was first observed on spheres by G. Eiffel [14]. It is a consequence of transition which causes the point of separation to move downstream, because, in the case of a turbulent boundary layer, the accelerating influence of the external flow extends further due to turbulent mixing. Hence the point of separation which lies near the equator for a laminar boundary layer moves over a considerable distance in the downstream direction. In turn, the dead area decreases considerably, and the pressure distribution becomes more like that for frictionless motion (Fig. 1.11). The decrease in the dead-water region considerably reduces the pressure drag, and that shows itself as a jump in the curve  $C_D = f(R)$ . L. Prandtl [26] proved the correctness of the preceding reasoning by mounting a thin wire ring at a short distance in front of the equator of a sphere. This causes the boundary layer to become artificially turbulent at a lower Reynolds number and the decrease in the drag coefficient takes place earlier than would otherwise be the case. Figs. 2.24 and 2.25 reproduce photographs of flows which have been made visible by smoke. They represent the subcritical pattern with a large value of the drag coefficient and the supercritical pattern with a small dead-water area and a small value of the drag coefficient. The supercritical pattern was achieved with Prandtl's tripping wire. The preceding experiment shows in a convincing manner that the jump in the drag curve of a circular cylinder and sphere can only be interpreted as a boundary-layer phenomenon. Other bodies with a blunt or rounded stern, (e. g. elliptic cylinders) display a type of relationship between drag coefficient and Reynolds number which is substantially similar. With increasing slenderness the jump in the curve becomes progressively less pronounced. For a streamline body, such as that shown in Fig. 1.12 there is no jump, because no appreciable separation occurs; the very gradual pressure increase on the back

of such bodies can be overcome by the boundary layer without separation. As we shall also see later in greater detail, the pressure distribution in the external flow exerts a decisive influence on the position of the transition point. The boundary layer is laminar in the region of pressure decrease, i. e. roughly from the leading edge to the point of minimum pressure, and becomes turbulent, in most cases, from that point onward throughout the region of pressure increase. In this connexion it is important to state that separation can only be avoided in regions of increasing pressure when the flow in the boundary layer is turbulent. A laminar boundary layer,

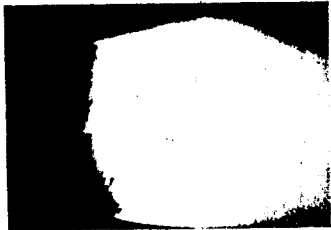


Fig. 2.24. Flow past a sphere at a subcritical Reynolds number; from Wieselsberger [39]

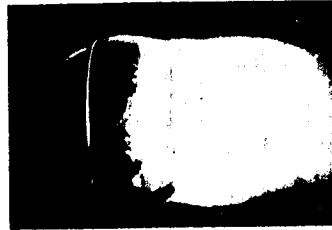


Fig. 2.25. Flow past a sphere at a supercritical Reynolds number; from Wieselsberger [39]. The supercritical flow pattern is achieved by the mounting of a thin wire ring (tripping wire)

as we shall see later, can support only a very small pressure rise so that separation would occur even with very slender bodies. In particular, this remark also applies to the flow past an aerofoil with a pressure distribution similar to that in Fig. 1.14. In this case separation is most likely to occur on the suction side. A smooth flow pattern around an aerofoil, conducive to the creation of lift, is possible only with a turbulent boundary layer. Summing up it may be stated that the small drag of slender bodies as well as the lift of aerofoils are made possible through the existence of a turbulent boundary layer.

**Boundary-layer thickness:** Generally speaking, the thickness of a turbulent boundary layer is larger than that of a laminar boundary layer owing to greater energy losses in the former. Near a smooth flat plate at zero incidence the boundary layer increases downstream in proportion to  $x^{0.8}$  ( $x$  = distance from leading edge). It will be shown later in Chap. XXI that the boundary-layer thickness variation in turbulent flow is given by the equation

$$\frac{\delta}{l} = 0.37 \left( \frac{U_{\infty} l}{\nu} \right)^{-1/5} = 0.37 (R_l)^{-1/5} \quad (2.9)$$

which corresponds to eqn. (2.2) for laminar flow. Table 2.1 gives values for the boundary-layer thickness calculated from eqn. (2.9) for several typical cases of air and water flows.

Table 2.1. Thickness of boundary layer,  $\delta$ , at trailing edge of flat plate at zero incidence in parallel turbulent flow

$U_{\infty}$  = free stream velocity;  $l$  = length of plate;  $\nu$  = kinematic viscosity

	$U_{\infty}$ [ft/sec]	$l$ [ft.]	$R_l = \frac{U_{\infty} l}{\nu}$	$\delta$ [in]
Air $\nu = 150 \times 10^{-6}$ ft <sup>2</sup> /sec	100	3	$2.0 \times 10^6$	0.73
	200	3	$4.0 \times 10^6$	0.64
	200	15	$2.0 \times 10^7$	2.30
	500	25	$8.3 \times 10^7$	2.90
	750	25	$1.25 \times 10^8$	2.68
Water $\nu = 11 \times 10^{-6}$ ft <sup>2</sup> /sec	5	5	$2.3 \times 10^6$	1.19
	10	15	$1.35 \times 10^7$	2.52
	25	150	$3.4 \times 10^8$	13.1
	50	500	$2.3 \times 10^9$	29.8

**Methods for the prevention of separation:** Separation is mostly an undesirable phenomenon because it entails large energy losses. For this reason methods have been devised for the artificial prevention of separation. The simplest method, from the physical point of view, is to move the wall with the stream in order to reduce the velocity difference between them, and hence to remove the cause of boundary-layer formation, but this is very difficult to achieve in engineering practice. However, Prandtl † has shown on a *rotating circular cylinder* that this method is very effective. On the side where the wall and stream move in the same direction separation is completely prevented. Moreover, on the side where the wall and stream move in opposite directions, separation is slight so that on the whole it is possible to obtain a good experimental approximation to perfect flow with circulation and a large lift.

Another very effective method for the prevention of separation is *boundary-layer suction*. In this method the decelerated fluid particles in the boundary layer are removed through slits in the wall into the interior of the body. With sufficiently strong suction, separation can be prevented. Boundary-layer suction was used on a circular cylinder by L. Prandtl in his first fundamental investigation into boundary-layer flow. Separation can be almost completely eliminated with suction through a slit at the back of the circular cylinder. Instances of the effect of suction can be seen in Figs. 2.14 and 2.15 on the example of flows through a highly divergent channel. Fig. 2.13 demonstrates that without suction there is strong separation. Fig. 2.14 shows how the flow adheres to the one side on which suction is applied, whereas from Fig. 2.15 it is seen that the flow completely fills the channel cross-section when the suction slits are put into operation on both sides. In the latter case the streamlines assume a pattern which is very similar to that in frictionless flow. In later years suction was successfully used in aeroplane wings to increase the lift. Owing to suction on the upper surface near the trailing edge, the flow adheres

† Prandtl-Tietjens: Hydro- and Aerodynamics. Vol. II, Tables 7, 8 and 9.

to the aerofoil at considerably larger incidence angles than would otherwise be the case, stalling is delayed, and much larger maximum-lift values are achieved [36].

After having given a short outline of the fundamental physical principles of fluid motions with very small friction, i. e. of the boundary-layer theory, we shall proceed to develop a rational theory of these phenomena from the equations of motion of viscous fluids. The description will be arranged in the following way: We shall begin in Part A by deriving the general Navier-Stokes equations from which, in turn, we shall derive Prandtl's boundary-layer equations with the aid of the simplifications which can be introduced as a consequence of the small values of viscosity. This will be followed in Part B by a description of the methods for the integration of these equations for the case of laminar flow. In Part C we shall discuss the problem of the origin of turbulent flow, i. e. we shall discuss the process of transition from laminar to turbulent flow, treating it as a problem in the stability of laminar motion. Finally, Part D will contain the boundary-layer theory for completely developed turbulent motions. Whereas the theory of laminar boundary layers can be treated as a deductive sequence based on the Navier-Stokes differential equations for viscous fluids, the same is not, at present, possible for turbulent flow, because the mechanism of turbulent flow is so complex that it cannot be mastered by purely theoretical methods. For this reason a treatise on turbulent flow must draw heavily on experimental results and the subject must be presented in the form of a semi-empirical theory.

#### References

- [1] Achenbach, E.: Experiments on the flow past spheres at very high Reynolds numbers. *JFM* 54, 565–575 (1972).
- [2] Berger, E., and Wille, R.: Periodic flow phenomena. *Annual Review of Fluid Mech.* 4, 313–340 (1972).
- [3] Berger, E.: Bestimmung der hydrodynamischen Größen einer Kármánschen Wirbelstrasse aus Hitzdrahtmessungen bei kleinen Reynolds-Zahlen. *ZFW* 12, 41–59 (1964).
- [3a] Bearman, P. W.: On the vortex shedding from a circular cylinder in the critical Reynolds number range. *JFM* 37, 577–585 (1969).
- [4] Blasius, H.: Grenzschichten in Flüssigkeiten mit kleiner Reibung. *Diss. Göttingen* 1907; *Z. Math. u. Phys.* 56, 1–37 (1908); Engl. transl. in *NACA TM* 1256.
- [5] Blenk, H., Fuchs, D., and Liebers, L.: Über die Messung von Wirbelfrequenzen. *Luftfahrtforschung* 12, 38–41 (1935).
- [6] Burgers, J. M.: The motion of a fluid in the boundary layer along a plane smooth surface. *Proc. First International Congress for Applied Mechanics*, Delft, 113–128 (1924).
- [7] Chang, P. K.: Separation of flow. Pergamon Press, Washington D.C., 1970.
- [8] Cermak, J. E.: Application of fluid mechanics to wind engineering -- A Freeman Scholar lecture. *Trans. ASME Fluids Engineering* 97, Ser. 1, 9–38 (1975); see also: Laboratory simulation of the atmospheric boundary layer. *AIAA J.* 9, 1746–1754 (1971).
- [8a] Cermak, J. E.: Aerodynamics of buildings. *Annual Review of Fluid Mech.* 8, 75–106 (1976).
- [9] Cermak, J. E., and Sadeh, W. Z.: Wind-tunnel simulation of wind loading on structures. Meeting Preprint 1417, ASCE National Structural Engineering Meeting, Baltimore, Maryland, 19–23 April, 1971.
- [10] Davenport, A. G.: The relationship of wind structure to wind loading. *Proc. Conference on Wind Effects on Buildings and Structures*, National Physical Laboratory, Teddington, Middlesex, Great Britain, 26–28 June 1963, Her Majesty's Stationary Office, London, Vol. 1, 54–112 (1965).

- [11] Domm, U.: Ein Beitrag zur Stabilitätstheorie der Wirbelstrassen unter Berücksichtigung endlicher und zeitlich wachsender Wirbelkerndurchmesser. *Ing.-Arch.* 22, 400–410 (1954).
- [12] Dubs, W.: Über den Einfluss laminarer und turbulenter Strömung auf das Röntgenbild von Wasser und Nitrobenzol. *Helv. phys. Acta* 12, 169–228 (1939).
- [13] Durgin, W. W., and Karlsson, S. K. F.: On the phenomenon of vortex street breakdown. *JFM* 48, 507–527 (1971).
- [14] Eiffel, G.: Sur la résistance des sphères dans l'air en mouvement. *Comptes Rendus* 155, 1597 (1912).
- [14a] Försching, H. W.: Aeroelastische Probleme an Hochbaukonstruktionen in freier Windumströmung. *Vulkan-Verlag, Essen, Haus der Technik, Part* 347, 3–18 (1976).
- [15] Frimberger, R.: Experimentelle Untersuchungen an der Kármánschen Wirbelstrasse. *ZFW* 5, 355–359 (1957).
- [16] Hansen, M.: Die Geschwindigkeitsverteilung in der Grenzschicht an der längsangeströmten ebenen Platte. *ZAMM* 8, 185–199 (1928); *NACA TM* 585 (1930).
- [17] van der Hegge Zijnen, B. G.: Measurements of the velocity distribution in the boundary layer along a plane surface. *Thesis Delft* 1924.
- [18] Heinemann, H. J., Lawaczek, O., and Bütefisch, K. A.: Kármán vortices and their frequency determination in the wakes of profiles in the sub- and transonic regime. *Symposium Transsonicum II Göttingen*, Sept. 1975. Springer Verlag, 1976, pp. 75–82; see also: *AGARD-Conférence Proc. No. 177*, Unsteady Phenomena in Turbomachinery (1975).
- [19] Hucho, W. H.: Einfluss der Vorderwagenform auf Widerstand, Giermoment und Seitenkraft von Kastenwagen. *ZFW* 20, 341–351 (1972).
- [20] von Kármán, Th.: Über den Mechanismus des Widerstandes, den ein bewegter Körper in einer Flüssigkeit erzeugt. *Nachr. Ges. Wiss. Göttingen, Math. Phys. Klasse* 509–517 (1911) and 547–556 (1912); see also *Coll. Works* 1, 324–338.
- [21] von Kármán, Th., and Rubach, H.: Über den Mechanismus des Flüssigkeits- und Luftwiderstandes. *Phys. Z.* 13, 49–59 (1912); see also *Coll. Works* 1, 339–358.
- [22] Lin, C. C.: On periodically oscillating wakes in the Oseen approximation. *R. v. Mises Anniversary Volume, Studies in Mathematics and Mechanics*. Academic Press, New York, 1950, 170–176.
- [23] Möller, E.: Luftwiderstandsmessungen am Volkswagen-Lieferwagen. *Automobiltechnische Z.* 53, 1–4 (1951).
- [23a] Novak, I.: Strouhal number of bodies and their systems (in Russian). *Strojnický Casopis* 26, 72–89 (1975).
- [24] Griffin, O. M., and Ramberg, S. E.: The vortex-street wakes of vibrating cylinders. *JFM* 66, 553–576 (1974).
- [25] Prandtl, L.: Über Flüssigkeitsbewegung bei sehr kleiner Reibung. *Proc. 3rd Intern. Math. Congr. Heidelberg* 1904, 484–491. Reprinted in: *Vier Abhandlungen zur Hydrodynamik und Aerodynamik*, Göttingen, 1927; see also *Coll. Works* 11, 575–584; Engl. transl. *NACA TM* 452 (1928).
- [26] Prandtl, L.: Der Luftwiderstand von Kugeln. *Nachr. Ges. Wiss. Göttingen, Math. Phys. Klasse*, 1914, 177–190; see also *Coll. Works* 11, 597–608.
- [27] Prandtl, L., and Tietjens, O.: *Hydro- und Aeromechanik* (based on Prandtl's lectures). Vol. 1 and 11. Berlin, 1929 and 1931; Engl. transl. by L. Rosenhead (Vol. 1) and J. P. den Hartog (Vol. 11), New York, 1934.
- [28] Relf, E. F., and Simmons, L. F. G.: The frequencies of eddies generated by the motion of circular cylinders through a fluid. *ARC RM* 917. London (1924).
- [29] Reynolds, O.: An experimental investigation of the circumstances which determine whether the motion of water shall be direct or sinuous, and of the law of resistance in parallel channels. *Phil. Trans. Roy. Soc.* 171, 935–982 (1883); see also *Scientific Papers* 2, 51.
- [30] Ribner, H. S., Etkins, B., and Neely, K. K.: Noise research in Canada: Physical and bio-acoustic. *Proc. First Int. Congress Aero. Sci. Madrid*, Pergamon Press, London, Vol. 1, 393–441 (1959).
- [31] Roshko, A.: Experiments on the flow past a circular cylinder at very high Reynolds number. *JFM* 10, 345–356 (1961).
- [32] Roshko, A.: On the development of turbulent wakes from vortex streets. *NACA Rep.* 1191 (1954).

- [32a] Rosenhead, L.: The formation of vortices from a surface of discontinuity. *Proc. Roy. Soc. A* 134, 170 (1931).
- [33] Rubach, H.: Über die Entstehung und Fortbewegung des Wirbelpaares bei zylindrischen Körpern. Diss. Göttingen 1914; VDI-Forschungsheft 185 (1916).
- [33a] Sarpkaya, T.: An inviscid model of two-dimensional vortex shedding for transient and asymptotically steady flow over an inclined plate. *JFM* 68, 109–128 (1975).
- [34] Sadeh, W.Z., and Cermak, J.E.: Turbulence effect on wall pressure fluctuations. *J. Eng. Mech. Div. ASCE* 98, No. EM 6, Proc. Paper 9445, 189–198 (1972).
- [35] Schlichting, H.: Aerodynamische Untersuchungen an Kraftfahrzeugen. Rep. Techn. Hochschule Braunschweig, 130–139 (1954).
- [36] Schrenk, O.: Versuche mit Absaugeflügel. *Luftfahrtforschung* XVI, 10–27 (1935).
- [37] Strouhal, V.: Über eine besondere Art der Tonerregung. *Ann. Phys. und Chemie, New Series* 5, 216–251 (1878).
- [38] Timme, A.: Über die Geschwindigkeitsverteilung in Wirbeln. *Ing.-Arch.* 25, 205–225 (1957).
- [38a] Wedemeyer, E.: Ausbildung eines Wirbelpaares an den Kanten einer Platte. *Ing.-Arch.* 30, 187–200 (1961).
- [39] Wieselsberger, C.: Der Luftwiderstand von Kugeln. *ZFM* 5, 140–144 (1914).

## CHAPTER III

Derivation of the equations of motion of  
a compressible viscous fluid

(Navier-Stokes equations)†

## a. Fundamental equations of motion and continuity applied to fluid flow

We shall now proceed to derive the equations of motion of a compressible, viscous, Newtonian fluid. In the general case of three-dimensional motion, the flow field is specified by the velocity vector

$$\mathbf{w} = i u + j v + k w$$

where  $u$ ,  $v$ ,  $w$  are the three orthogonal components, by the pressure  $p$ , and by the density  $\rho$ , all conceived as functions of the coordinates  $x$ ,  $y$ ,  $z$ , and time  $t$ . For the determination of these five quantities there exist five equations: the continuity equation (conservation of mass), the three equations of motion (conservation of momentum) and the thermodynamic equation of state  $p = f(\rho)$ .‡

The equation of continuity expresses the fact that for a unit volume there is a balance between the masses entering and leaving per unit time, and the change in density. In the case of non-steady flow of a compressible fluid this condition leads to the equation:

$$\frac{D\rho}{Dt} + \rho \operatorname{div} \mathbf{w} = \frac{\partial \rho}{\partial t} + \operatorname{div}(\rho \mathbf{w}) = 0, \quad (3.1)$$

whereas for an incompressible fluid, with  $\rho = \text{const}$ , the equation of continuity assumes the simplified form

$$\operatorname{div} \mathbf{w} = 0. \quad (3.1a)$$

The symbol  $D\rho/Dt$  denotes here the substantive derivative which consists of the local contribution (in non steady flow)  $\partial\rho/\partial t$ , and the convective contribution (due to translation),  $\mathbf{w} \cdot \operatorname{grad} \rho$ .

† In the Sixth Edition this chapter has been revised by the Translator at the Author's invitation.  
‡ If the equation of state contains temperature as an additional variable, a further equation is supplied by the principle of the conservation of energy in the form of the First Law of Thermodynamics; cf. Chap. XII.